

# Study of drying kinetics and moisture diffusivity in iron ore briquettes after using different drying techniques

R. Sharma \*, D.S. Nimaje

Department of Mining Engineering, National Institute of Technology, Rourkela, India, 769008

(Received 10 September 2024; Accepted 24 June 2025)

## Abstract

*This study aimed to investigate the drying kinetics, effective moisture diffusivity and thermal degradation properties of iron ore briquettes using hot air drying, microwave drying, and infrared drying methods. The results showed that both hot air and infrared drying processes are gradual, starting with the drying of the outer surface and gradually moving toward the inner core of the briquette. In microwave drying, the iron ore briquette is heated from the inside out. Moisture diffusivity is moderate at 100W, lower at 180W, and very high at 300W. For both hot air and infrared drying, moisture diffusivity is low at 105°C, and maximum strength is observed at 120°C. Compressive strength analysis was performed after applying different drying techniques with the highest strength of 4.195 N/mm<sup>2</sup> recorded at 120°C in the infrared chamber. The drying kinetic curves for hot air, microwave, and infrared methods were analyzed using five different moisture ratio (MR) models: Newton, Henderson and Pabis, Logarithmic, Diffusion, and Wang & Singh. This research will offer valuable insights into the degradation of iron ore briquettes following the optimal removal of approximately 90% of moisture from the sample. This approach will also guide the production of high-quality dried products and assist in producing green briquettes with reduced carbon emissions. In this work, heat induration is employed for drying, as opposed to techniques like sintering and nodulizing, which involve heating agglomerates at high temperatures approximately 1100 °C and result in higher carbon emissions.*

**Keywords:** Moisture diffusivity; Iron ore briquette; Drying kinetics; Compressive strength

## 1. Introduction

The infrastructure, vehicle, weapon and space industries all rely heavily on raw materials supplied by the steel industry. As iron ore, the primary component in steel production is rapidly being depleted it's crucial to use this resource more efficiently. In metal mines conventional drilling and blasting methods are used because hard rock cutting machines like shearers are not suitable. This lack of selective mining leads to the generation of a significant amount of fines. Continuous mineral deposits are rare and those that do exist in metal mines tend to be relatively small in shape and size [1]. Cutting machines are not suitable for use in metal mines due to the hardness of the host rock unlike in softer rocks such as coal where selective mining is feasible. The conventional method of drilling and blasting is commonly used for mining operations. Due to the mostly discontinuous nature of iron ore deposits, blasting generates many fragments resulting in the production of substantial amounts of iron ore fines in addition to lump iron ore. Additionally, various iron ore beneficiation processes produce both macro and micro iron ore fines [2]. Previously, lump iron ore was used in blast furnaces to produce pig iron and slag which were then used to make steel. To efficiently utilize the large quantities of iron ore fines generated

---

Corresponding author: [rishi32122@gmail.com](mailto:rishi32122@gmail.com)

during mining iron ore agglomeration is used in steel production. Pelletizing a key agglomeration process enhances blast furnace productivity and is essential in steel manufacturing. During this process, the material is primarily formed into balls or agglomerated with a binder and water capillaries forming between the grains of the iron ore briquette [3]. The agglomeration of metallurgical wastes such as flue dust and LD (Linz-Donawitz) sludge was combined with iron ore fines, bentonite, and cement which acted as a binder [4]. Traditionally, iron ore lumps were used in the blast furnace to produce molten iron which was then mixed with carbon to create steel. The reduction characteristics of the blast furnace were enhanced by spreading coking coal powder over the lump iron ore which facilitated the reduction of the iron ore. Iron ore is typically found in narrow veins beneath the earth's surface. In the 1950s, the steel industry began agglomerating iron ore fines to use as feed for blast furnaces [5]. Iron ore fines were formed into briquettes using various binders, including bentonite, cement, starch, and molasses. The agglomerates of iron ore fines are more porous as compared to lump iron ores this helps in achieving good reduction characteristics [6]. The binders such as bentonite provide initial green strength to the briquette while cement helps further strengthen the agglomerate after open air drying [7]. Bentonite is hygroscopic and has a high water absorption capacity. When hydrated, it expands and forms a bonding layer around the iron ore particles holding them together [8]. The bentonite particles create individual platelets that coat the iron ore particles, aiding in their bonding. As moisture begins to evaporate during open air drying bentonite develops a fibrous matrix that effectively binds the iron ore particles together [9].

Agglomerates created with an appropriate binder must have sufficient strength to prevent premature disintegration in the blast furnace [10]. If iron ore briquettes disintegrate prematurely their reduction efficiency decreases. Iron ore mining typically employs conventional drilling and blasting methods which produce three types of ore: coarse-size ore (lump ore), medium-size ore (sinter feed), and fine-size ore (pellet feed). The moisture content of fine ore should be carefully optimized to prevent ore loss during handling and transportation. Proper drying techniques are essential to achieve this optimization, as ore with high moisture content can lead to transportation issues. Agglomeration was also achieved through the sintering process where iron ore fines, coke fines, and biomass were mixed and heated to high temperatures. This process produces a solid porous material known as sinter. During the sintering process, the ignition temperature of the agglomeration charge must be carefully controlled and optimized by gradually cooling the sinter beds. The sintering reaction primarily begins at the contact points between the fines and fluxes where solid reactions produce the initial primary melt. Large particles are often inactive due to their large surface area [11]. Sintering can be performed using both solid fuel combustion and secondary gas injection. The gaseous fuel is injected in pulse mode to meet the energy requirements of the sinter feed bed. When sinter feed is introduced into the blast furnace various gases are employed to accelerate the reduction process. In the European steel industry gases such as nitrogen oxide, sulfur dioxide and carbon dioxide are used to enhance reduction efficiency [12]. Agglomeration plants utilize various dryers to maintain the initial strength of green pellets during transportation and handling. The moisture content of the agglomerate also affects its quality when supplied for direct reduction in the blast furnace [13]. Iron ore pellets produced in the agglomeration industry can be customized to meet customer specifications. The moisture content, size, and strength of the pellets can be adjusted according to industry requirements.

The drying process can enhance pellet quality but it is both time-consuming and energy intensive. The straight kiln or grate kiln drying method involves passing pellet beds through several zones: drying, preheating, firing, and cooling. The moving grate loaded with the pellet bed moves through the drying and preheating zones. Convective air is circulated through the pellet bed with a rotary kiln used in the firing zone. During up-draught drying warm air is passed through the pellet bed from below while in down-draught drying it is introduced from above [14]. After passing through the drying zone the moving grate enters the rotary kiln where pre-heated gas at 1000°C is introduced from below. When the pellets exit the kiln they become hardened and are then transferred to an annular cooler. The cooling zone is divided into three basic sections, with cold air blown into each section to remove excess heat from the pellets [15]. Pelletization is a type of agglomeration process that requires optimization of physical, chemical, and metallurgical characteristics for the steelmaking industry [16]. The iron rich dust briquette was produced using cold briquetting technology, incorporating blast furnace dust, iron dust, and portland cement. The drying kinetics of the briquette were examined under the high-temperature conditions of a blast furnace. In the reducing atmosphere of blast furnace, iron rich dust briquette undergoes different stages of reduction in mechanical strength of briquettes. The mechanical strength of the briquette decreases with the increase of reduction degree and metallization rate, from 4.58 KN at 100 °C to 0.52 KN at 1100 °C [17]. The handling and transportation of iron ore concentrates was optimized by studying the drying kinetics of iron ore concentrates. The different properties of pellet feed were also studied for proper designing of drying operation for the agglomeration plant [13]. Sponge iron plants commonly utilize coal-based reduction processes for iron ore briquettes. In this study, iron ore-carbon briquettes were prepared using hematite and biochar fines, with reduction carried out in a CO-CO<sub>2</sub> reducing atmosphere. Drying model predictions based on experimental results demonstrated improvement in reduction efficiency. The carbon in the briquette enhances the reduction degree of the iron ore briquette by facilitating both the reduction of iron oxide and the prevention of metallic iron re-oxidation [18].

The peak load-bearing capacity of iron ore briquettes tends to decline at elevated temperatures around 1300°C, primarily due to the degradation of the starch binder [19]. Employing low-temperature drying methods can improve briquette strength, thereby enhancing their durability during handling, storage, and transportation without compromising structural integrity. Operational insights from blast furnace usage indicate that a compressive strength of approximately 3.43 MPa is sufficient to ensure reliable performance during storage and handling, while also minimizing dust generation [20].

Open-air drying is generally inadequate for imparting the necessary strength to briquettes, highlighting the importance of controlled drying methods. Seasonal factors such as the rainy season can further hinder natural drying, necessitating the use of alternative drying techniques. Therefore, optimizing these methods is essential to determine the most effective approach for achieving the desired briquette strength [21]. Hot air oven drying initiates moisture removal from the outer surface of the briquette and gradually progresses inward [19]. In contrast, microwave drying heats the material internally, driving moisture from the core to the surface, which can result in internal cracking and reduced structural integrity [22, 23]. Infrared drying, on the other hand, applies heat externally and allows for more gradual and uniform moisture reduction, which can contribute to improved briquette strength [11].

Iron ore agglomeration plants must use various conventional drying techniques, such as coal briquette dryers, tunnel dryers, microwave heating dryers and conventional heating dryers to ensure the iron ore briquettes are properly dried. This prevents breakage during handling, storage and transportation [24]. This study demonstrates that the use of iron ore briquettes can enhance the production efficiency of blast furnaces. The approach supports the generation of high-quality dried briquettes while promoting environmentally friendly practices through reduced carbon emissions. The incorporation of metallurgical wastes such as LD sludge and flue dust—both rich in iron oxide—further boosts blast furnace performance. Additionally, the carbon content in flue dust facilitates the carbothermic reduction of iron ore, thereby improving the overall process efficiency. The utilization of these industrial by-products not only enhances operational efficiency but also significantly lowers waste disposal costs for the steel industry. Unlike traditional agglomeration techniques such as sintering and nodulizing, which require high-temperature processing around 1100°C and result in substantial carbon emissions [12]. This study employs low-temperature drying methods. These alternative low temperature drying processes reduce environmental impact by minimizing energy consumption and lowering greenhouse gas emissions during briquette production. These techniques must be optimized for both cost and quality to produce high quality iron ore briquettes suitable for blast furnaces. It will also aid in producing high-quality dried products and help in manufacturing green briquettes with lower carbon emissions.

## **2. Material and Methods**

### **2.1 Materials**

The composition used for preparing iron ore briquettes consists of LD sludge (47.2%), flue dust (28.3%), iron ore fines (16.5%), cement (6%), and bentonite (2%). To form the briquettes, iron ore fines are mixed with metallurgical wastes, such as LD sludge and flue dust. Cement and bentonite are added as binders to help shape the briquettes into a cylindrical form. The resulting samples have a diameter of 3 cm and a height of 4 cm.

### **2.2 Methods**

The hot air oven, microwave, and infrared drying methods are employed to provide initial strength to freshly prepared briquettes, making them suitable for handling, storage, and transportation.

**Hot air oven drying:** A universal hot air oven is used to dry the briquettes from the outside inwards, allowing for gradual drying. This method results in briquettes with good stability and quality.

**Microwave drying:** A microwave oven (Samsung CE73JD model) is used to dry the iron ore briquettes from the inside outwards. This method can lead to the generation of cracks, negatively impacting the quality of the briquettes.

**Infrared drying:** An infrared dryer (Twin Engineering model) was used to heat the iron ore briquettes. The infrared chamber is equipped with six lamps, each with a wattage of 1 kW. The briquettes are gradually heated from the outside to the inside, maintaining their quality throughout the process.

**Compressive strength test:** A medium-range universal testing machine (H10KS) with a capacity of 10 kN was used to assess the compressive strength of various laboratory-produced agglomerates. The iron ore briquettes were stored at room temperature for seven days and then dried at different temperatures using various drying methods. A compression test was conducted to determine which drying method results in the highest strength.

**Scanning Electron Microscopy (SEM):** SEM image analysis was performed to identify the various elements present in cement, bentonite, flue dust, LD sludge, and iron ore fines. Before the analysis, the powder samples were coated to eliminate any traces of external moisture. The experiment was conducted using the Japan Electron Optics Limited JSM-6480LV model. The SEM images were also used to determine the degree of inter particle fiber bonding in the iron ore briquettes after drying with different techniques.

### 3. Results and Discussion

#### 3.1 Selection of briquette composition

The iron ore briquettes were prepared using four different compositions by varying the binder concentration in the base composition (Table 1). The curing of the briquette was done in the open air for 24 h. A compressive strength test was conducted on different compositions using a Universal testing machine (H10KS medium range). The Composition (Iron ore fines (16.5%), LD sludge (47.2%), Flue dust (28.3%), Bentonite (2%) and Cement (6%)) with the highest strength (0.476 MPa) was selected for further experimentation (Figure 1).

**Table 1.** Different compositions prepared for compressive strength test

Composition	Bentonite %	LD Sludge %	Iron ore fines %	Flue dust %	Cement %
1	1.5	49.2	16.5	28.3	4.5
2	1.75	47.2	17.5	28.3	5.25
3	2	47.2	16.5	28.3	6
4	2.5	47.2	16.5	26.3	7.5

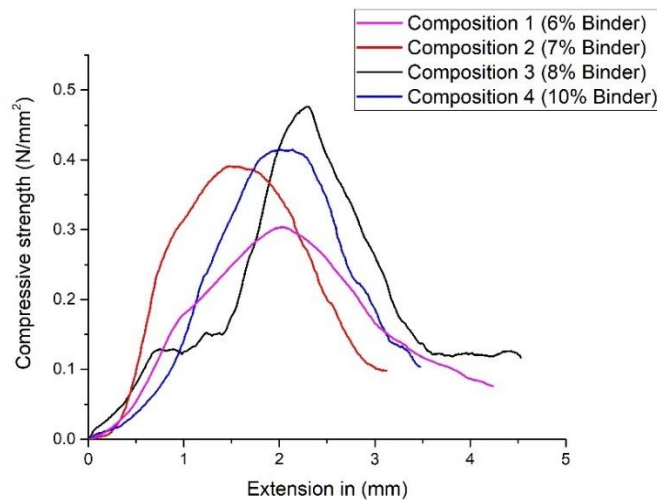


**Figure 1.** Graph between compressive strength and extension for different compositions

The compressive strength test conducted on the seventh day revealed that iron ore briquettes achieved maximum strength due to nearly negligible moisture content. The iron ore briquette was also subjected to open air drying for seven days without using any kind of drying techniques. The strength value of 1.85 MPa was observed after open air drying of briquette for seven days without using any initial curing methods (Figure 2).

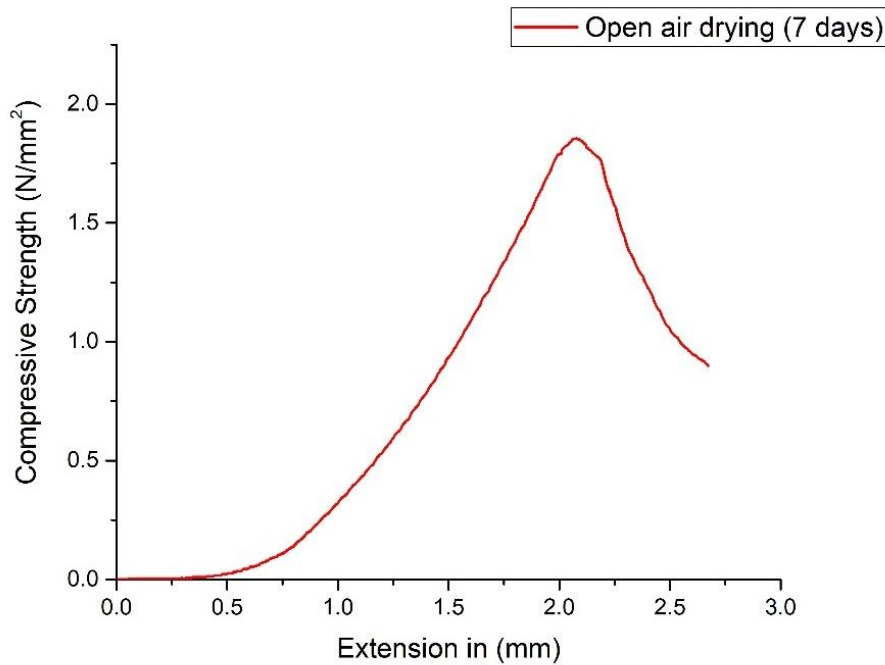


**Figure 2.** Strength analysis after storage of iron ore briquette in open air for seven days

The iron ore briquettes were initially dried using hot air drying, and after seven days of open-air storage, an improvement in strength was observed compared to briquettes dried solely in open air. This underscores the importance of employing an efficient drying technique for iron ore briquettes. Therefore, various drying methods were explored to determine the most effective approach for enhancing briquette strength.

### **3.2 Compressive Strength Analysis**

The compressive strength analysis on the seventh day revealed that the iron ore briquettes reached maximum strength, likely due to the minimal moisture content. The briquettes were dried using hot air and infrared methods at temperatures of 105°C, 110°C, 120°C, 130°C, and 140°C. The strength of the iron ore briquettes after seven days of storage in an open-air environment was compared with their extension, which indicates the deformation or strain during the compression test, to determine the briquette with the highest strength (Figures 3 and 5). The strength of the briquettes increased up to 120°C for both hot air (3.680 N/mm<sup>2</sup>) and infrared (4.195 N/mm<sup>2</sup>) drying methods but began to decrease at 130°C and 140°C.

The iron ore briquettes were dried using microwave drying at power levels of 100W, 180W, and 300W. After seven days of storage in an open air environment, their strength was compared to determine which briquette had the highest strength. The briquettes dried at 100W showed the highest strength (2.884 N/mm<sup>2</sup>). However, the strength decreased at 180W and 300W due to the breakage of inter particle bonding within the briquettes (Figure 4).

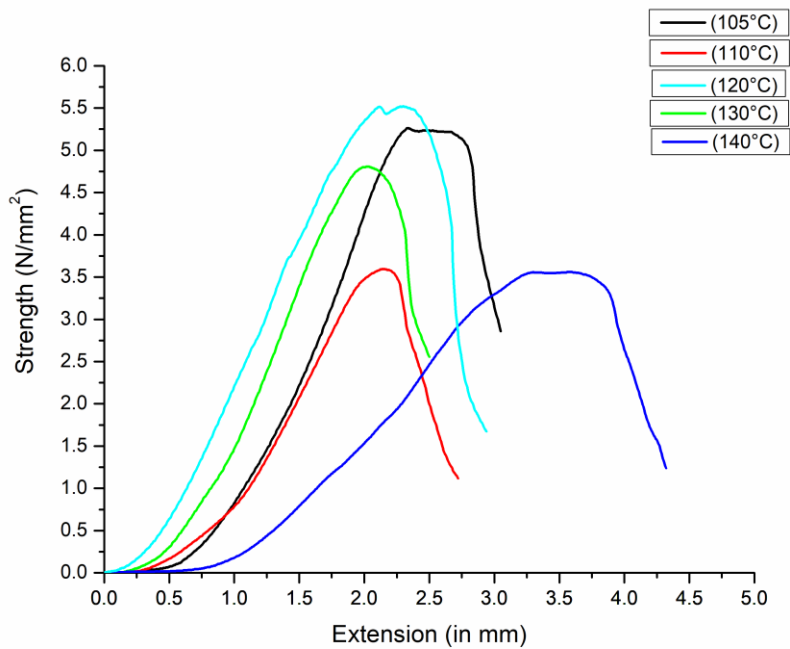


**Figure 3.** Strength analysis after hot air drying and seven days of storage

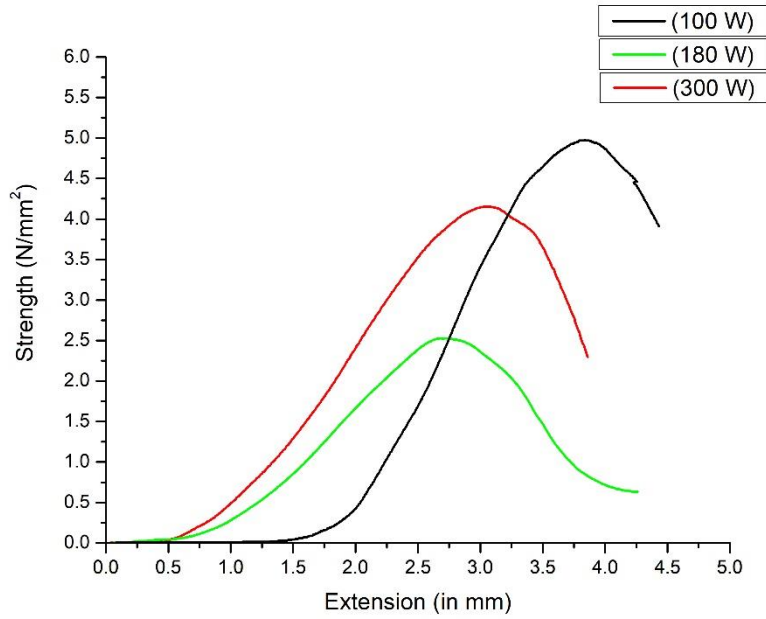


**Figure 4.** Strength analysis after microwave drying and seven days of storage

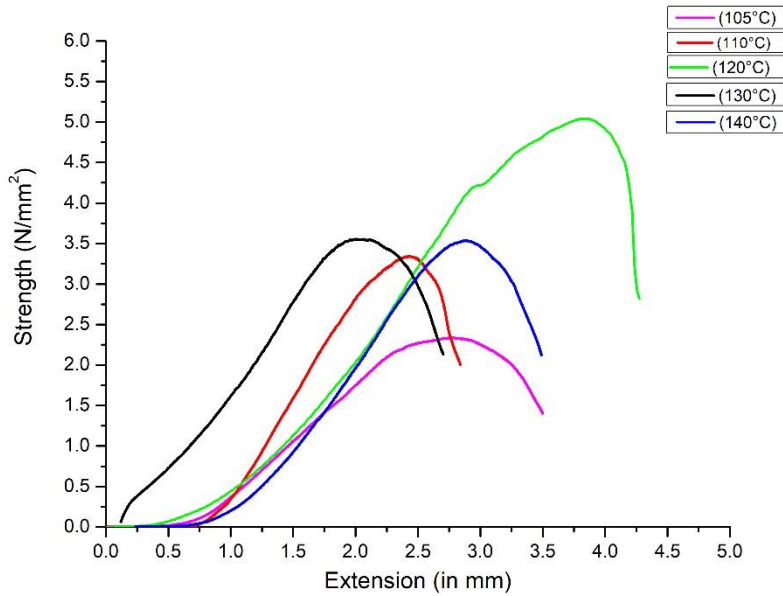


**Figure 5.** Strength analysis after infrared drying and seven days of storage

### 3.3 SEM Image Analysis

#### 3.3.1. SEM Image Analysis After Hot Air Drying

The analysis showed the presence of fiber bonds at temperatures of 105°C, 110°C, and 120°C, with the maximum number of bonds observed at 120°C, resulting in the highest strength (3.680 N/mm<sup>2</sup>) after hot air drying (Figures 6-9).

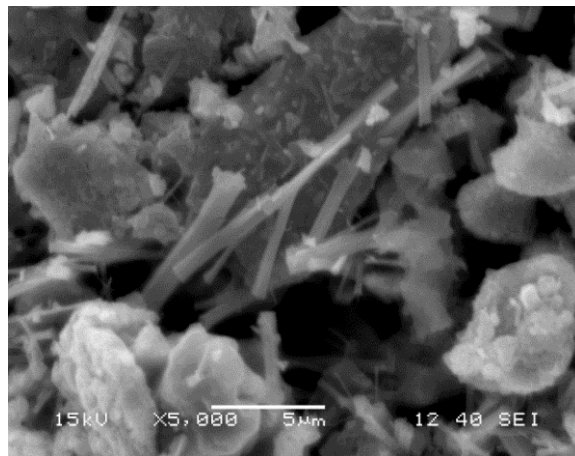


**Figure 6.** SEM image analysis after hot air drying at 105°C and seven days of storage

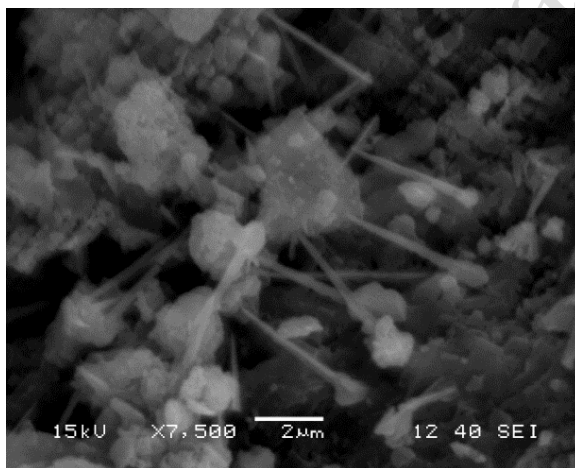


**Figure 7.** SEM image analysis after hot air drying at 110°C and seven days of storage

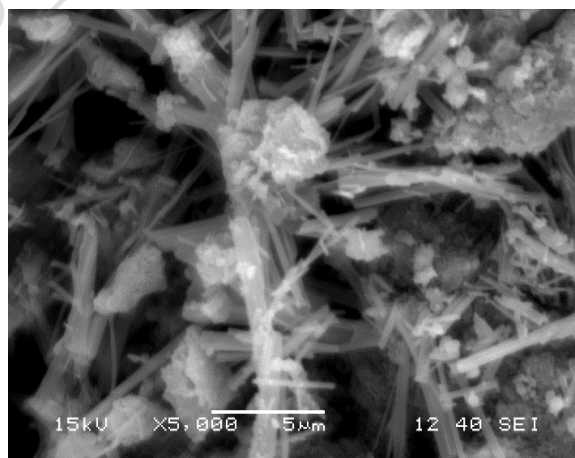


**Figure 8.** SEM image analysis after hot air drying at 120°C and seven days of storage

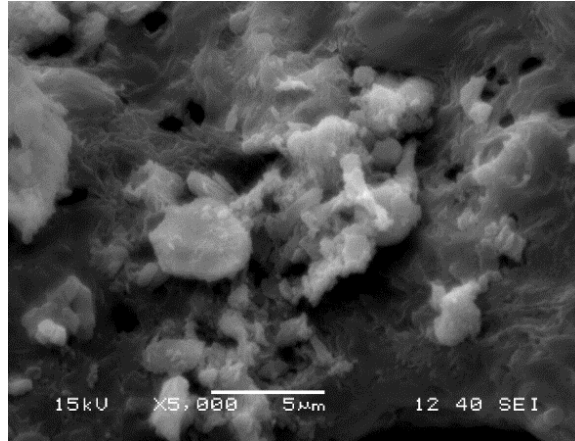


**Figure 9.** SEM image analysis after hot air drying at 130°C and seven days of storage

### 3.3.2 SEM Image Analysis After Microwave Drying

Fiber bonds were present at power levels of 100W, 180W, and 300W, with the maximum number of bonds observed at 100W, resulting in the highest strength (2.884 N/mm<sup>2</sup>) after microwave drying (Figures 10-12).

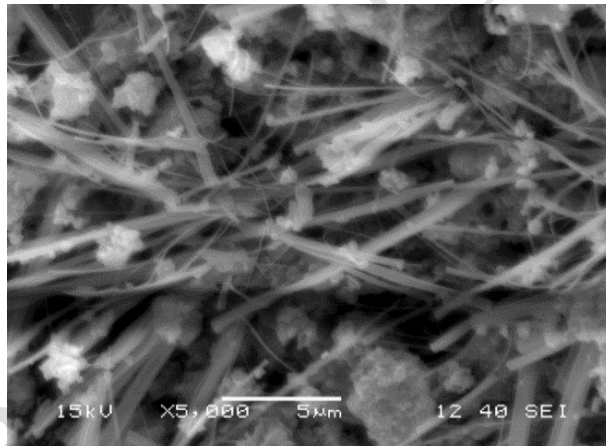


**Figure 10.** SEM image analysis after microwave drying at 100 W and seven days of storage

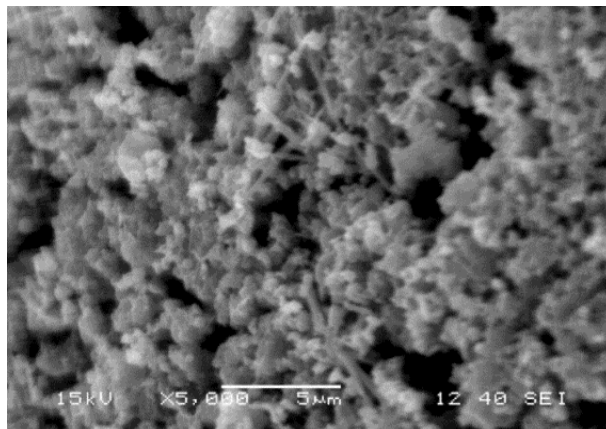


**Figure 11.** SEM image analysis after microwave drying at 180 W and seven days of storage

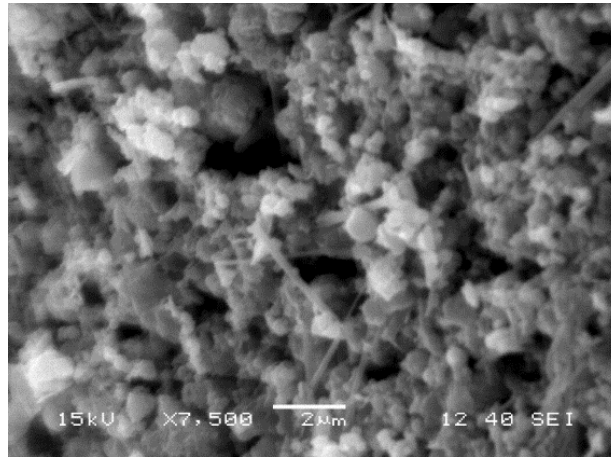


**Figure 12.** SEM image analysis after microwave drying at 300W and seven days of storage

### 3.3.3 SEM Image Analysis After Infrared Drying

SEM image analysis revealed the presence of fiber bonds at temperatures of 105°C, 110°C and 120°C with the maximum bonding observed at 120°C resulting in the highest strength (4.195 N/mm<sup>2</sup>) after infrared drying (Figures 13-16).

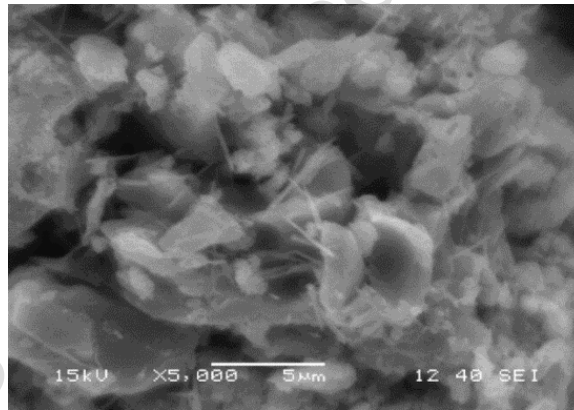


**Figure 13.** SEM image analysis after infrared drying at 105°C and seven days of storage

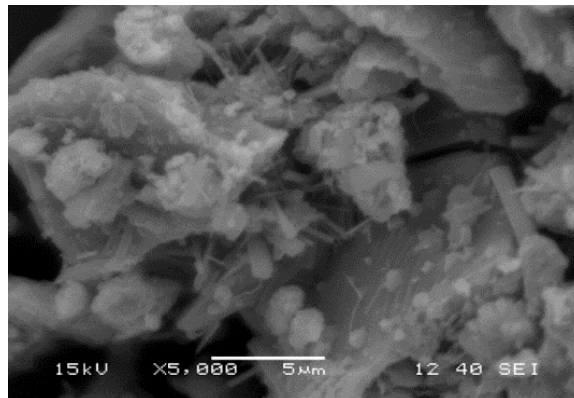


**Figure 14.** SEM image analysis after infrared drying at 110°C and seven days of storage

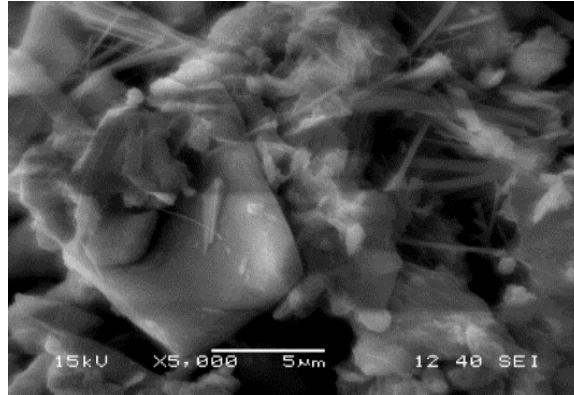


**Figure 15.** SEM image analysis after infrared drying at 120°C and seven days of storage

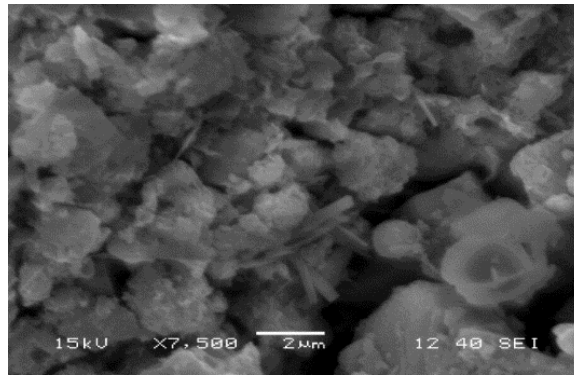


**Figure 16.** SEM image analysis after infrared drying at 130°C and seven days of storage

### **3.4 Comparative Analysis of the Strength of Different Drying Techniques**

The briquettes were dried using hot air and infrared methods at temperatures of 105°C, 110°C, 120°C, 130°C and 140°C, while microwave drying was conducted at power levels of 100W, 180W, and 300W. After seven days of storage in an open-air environment, their compressive strength was evaluated to identify the optimal drying condition. The highest strength for both hot air and infrared drying was observed at 120°C, while microwave drying yielded the best results at 100W. These optimal conditions were then compared to determine the most efficient drying technique.

Graphical analysis of the strength of iron ore briquettes dried using hot air, microwave, and infrared methods reveals that infrared drying yields the highest strength at 120°C (4.195 N/mm<sup>2</sup>) compared to microwave and hot air drying. Microwave drying results in the lowest strength at 100W (2.884 N/mm<sup>2</sup>) because it heats the briquette from the inside out, causing moisture to flow outward and generating numerous cracks. Hot air drying heats the briquette from the exterior surface to the interior at a slower rate, producing stable briquette but with less strength (3.680 N/mm<sup>2</sup>) as compared to infrared drying (Figure 17).

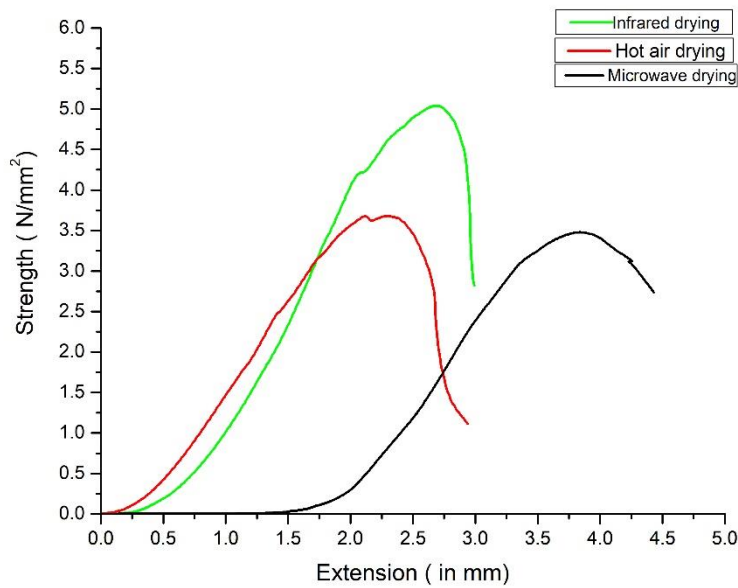


**Figure 17.** Strength analysis after hot air, microwave & infrared drying and seven days of storage

### 3.5 Drying Kinetics of Iron Ore Briquette Using Different Drying Techniques

The kinetic curves for hot air, microwave and infrared drying were fitted using five different moisture ratio (MR) models: Newton, Henderson and Pabis, Logarithmic, Diffusion and Wang & Singh. These commonly applied models for various products were evaluated based on the coefficient of determination ( $R^2$ ). A drying model is deemed optimal for predicting moisture variation during drying when its  $R^2$  value approaches 1, indicating a strong correlation between the predicted and actual data. Drying models with  $R^2$  value closer to 1 and the least RMSE (Root mean square error) will be selected as the drying model most suitable for different drying techniques (Table 4-5).

#### 3.5.1 Theoretical basis of using different drying models

The Newton Model is the simplest form of an exponential drying model, assuming that the drying rate is directly proportional to the remaining moisture content. It is commonly used as an initial approach for analyzing drying data. This model is particularly suitable for situations where external moisture diffusion is the dominant mechanism, typically during the constant drying rate period. Its simplicity makes it easy to apply and interpret.

The Henderson and Pabis Model builds on the Newton Model by introducing a scaling factor,  $a$ , which enhances its flexibility and allows for a better fit to experimental data. This model is particularly effective for materials that exhibit more complex drying behavior. Although empirical in nature, it is based on the principles of exponential decay and is widely used for drying studies involving agricultural and mineral materials.

The Logarithmic Model introduces a constant term to the exponential equation, enhancing its ability to represent moisture equilibrium and the gradual decrease in drying rate toward the end of the process. This makes it particularly effective for capturing the slower drying behavior observed during the falling rate period. It provides a strong empirical fit for porous materials, such as briquettes.

The Wang and Singh Model is a purely empirical polynomial model. It often provides a good fit within specific time intervals. This model is especially useful in situations where traditional drying models fail to accurately describe the drying behavior.

The Diffusion Model, based on Fick's second law, describes internal moisture movement within porous solids. As a physically based model, it provides a detailed understanding of how moisture diffuses through the material. It is especially useful for calculating the effective moisture diffusivity and is crucial for analyzing internal mass transfer limitations in materials like iron ore briquettes.

The selection of these five models is primarily guided by the following considerations:

#### 1. Material properties of iron ore briquettes

- Iron ore briquettes are compacted but retain some porosity, affecting internal moisture movement.
- Capillary action and vapor diffusion dominate internal moisture transport.
- Heterogeneity due to the mix of iron ore fines, LD sludge, flue dust, and binders like bentonite and cement.

#### 2. Drying mechanisms

- Hot air drying involves convective heat transfer and evaporative mass transfer.
- Microwave drying heats internally via dielectric heating, causing rapid moisture migration from within.
- Infrared drying transfers heat primarily through radiation, leading to surface heating and deeper penetration compared to convection.

#### 3. Heat and mass transfer laws

- Fick's second law of diffusion governs internal moisture movement in porous solids.
- Newton's law of cooling is the basis for exponential-type models (like Newton and Henderson & Pabis).
- Models are often semi-theoretical or empirical, designed to approximate real-world drying behaviours without full analytical solutions.

*Relevance of drying models to iron ore briquette drying:* The selected drying models range from simple to more complex formulations (Newton → Wang & Singh), each representing different aspects of the drying process. The Newton and Henderson & Pabis models are typically effective during the falling rate period of drying. The Logarithmic and Diffusion models are better suited

for scenarios involving multiple moisture transport mechanisms. The Wang & Singh model is particularly applicable to microwave drying, where internal heat generation results in non-exponential moisture loss. All these models are computationally efficient and require relatively few parameters, making them practical choices for fitting experimental data without adding undue complexity. The theoretical background and specific relevance of each model to the drying of iron ore briquettes are summarized in Table 2.

**Table 2. Theoretical Basis and Relevance of Selected Models**

Model	Theoretical Basis	Relevance to Iron Ore Briquette Drying
Newton	Based on Newton's cooling law	Simplest model; assumes constant drying rate and surface evaporation
Henderson & Pabis	Modification of Newton's model	Introduces a scaling factor (a), accounts for sample shape and surface area
Logarithmic	Empirical model; extension of Henderson	Captures more complexity (residual moisture or secondary mechanisms)
Diffusion (Fickian)	Based on Fick's second law	Represents internal moisture diffusion, suited to thick or porous samples
Wang & Singh	Empirical polynomial	Does not assume exponential decay; useful for non-linear drying behavior like microwave drying

The advantages and limitations of the selected drying models are summarized in Table 3. These models were chosen over more complex alternatives because they offer a good balance between physical interpretability and fitting accuracy. While advanced models such as Page, Two-term, or Midilli may provide higher precision, they often involve additional parameters that can lead to unstable or non-unique fitting, especially with limited datasets. The five selected models are well-established in drying research, facilitating comparability across studies and simplifying model validation. Their effectiveness can be quantitatively assessed using statistical indicators such as the coefficient of determination ( $R^2$ ), root mean square error (RMSE) allowing for an objective evaluation of the most appropriate model for each drying technique.

**Table 3. Advantages and Disadvantages**

Model	Advantages	Disadvantages
Newton	Simple; easy to use; interpretable	Oversimplifies; does not account for internal resistance
Henderson & Pabis	Better than Newton for real systems; accounts for geometry	Still limited in capturing multi-phase drying
Logarithmic	Good for materials with residual moisture plateau	More parameters; may not represent physics clearly
Diffusion	Physically meaningful; suited for thick or porous materials	Assumes uniform initial moisture and simple geometry
Wang & Singh	Flexible; fits nonlinear drying well (e.g., microwave)	Entirely empirical; not based on physical laws

### 3.5.2. Model Fitting Analysis of Different Drying Models

The selection of appropriate moisture ratio (MR) models to fit the drying kinetics of iron ore briquettes is essential to accurately describe the drying behavior and predict the moisture content over time. The theoretical basis for selecting Newton, Henderson and Pabis, Logarithmic, Diffusion, and Wang & Singh models lies in their ability to simulate different aspects of heat and

mass transfer during drying processes. These models are particularly useful for materials like iron ore briquettes, which have complex porous structures, varying thermal properties, and distinct moisture transport mechanisms.

The Root Mean Square Error (RMSE) was calculated in MATLAB to quantitatively assess the deviation between predicted and observed moisture ratio (MR) values. RMSE was used alongside  $R^2$  to select the most accurate drying model. The Root Mean Square Error (RMSE) serves as an important metric for assessing overall model accuracy, with lower RMSE values indicating a closer fit between experimental and predicted data. In MATLAB, curve fitting was conducted using built-in optimization functions aimed at minimizing RMSE during parameter estimation. To ensure data reliability before model fitting, specific screening criteria were applied. Only moisture ratio values from datasets with consistent initial moisture content (within  $\pm 5\%$  across replicates) were considered. Time points affected by inconsistent heating such as during the warm-up phase or due to system disturbances were excluded. Additionally, any measurements impacted by instrument error or sensor instability were removed from the analysis.

**Table 4.** Coefficients of different drying models and RMSE for iron ore briquette samples under different temperatures of hot air and infrared drying

Model	Equation	Temperatures (°C)	R <sup>2</sup> Value	RMSE	R <sup>2</sup> Value	RMSE
			Hot air drying		Infrared drying	
Newton	$MR = \exp(-kt)$	105	0.9856	0.0319	0.9452	0.0562
		110	0.9880	0.0296	0.9505	0.0535
		120	0.9866	0.0319	0.9569	0.0507
		130	0.9875	0.0307	0.9478	0.0544
		140	0.9808	0.0384	0.9538	0.0533
Henderson and Pabis	$MR = a \cdot \exp(-kt)$	105	0.9857	0.0324	0.9503	0.0544
		110	0.9887	0.0294	0.9579	0.0502
		120	0.9875	0.0316	0.9631	0.0478
		130	0.9876	0.0313	0.9586	0.0493
		140	0.9809	0.0393	0.9592	0.0511
Logarithmic	$MR = a \cdot \exp(-kt) + c$	105	0.9961	0.0173	0.9950	0.0175
		110	0.9952	0.0195	0.9981	0.0110
		120	0.9943	0.0218	0.9984	0.0101
		130	0.9941	0.0220	0.9991	0.0075
		140	0.9932	0.0241	0.9985	0.0100
Wang and Singh	$MR = 1 + at + bt^2$	105	0.9911	0.0173	0.9749	0.0433
		110	0.9940	0.0213	0.9589	0.0715
		120	0.9930	0.0237	0.9632	0.0593
		130	0.9894	0.0289	0.9894	0.0167
		140	0.9907	0.0273	0.9907	0.0134
Diffusion	$MR = a \cdot \exp(-kt) + (1 - a) \exp(-kbt)$	105	0.9952	0.0191	0.9938	0.0107
		110	0.9940	0.0218	0.9970	0.0053
		120	0.9935	0.0232	0.9665	0.0540
		130	0.9877	0.0319	0.9643	0.0589
		140	0.9810	0.0403	0.9977	0.0036

**Table 5.** Coefficients of different drying models and RMSE for iron ore briquette sample under different

*temperatures of microwave drying*

Model	Equation	Wattages (W)	R <sup>2</sup> value	RMSE
Newton	$MR = \exp(-kt)$	100	0.9796	0.0425
		180	0.9749	0.0473
		300	0.9729	0.0522
Henderson and Pabis	$MR = a \cdot \exp(-kt)$	100	0.9871	0.0346
		180	0.9843	0.0384
		300	0.9818	0.0445
Logarithmic	$MR = a \cdot \exp(-kt) + c$	100	0.9871	0.0355
		180	0.9843	0.0394
		300	0.9832	0.0447
Wang and Singh	$MR = 1 + at + bt^2$	100	0.9929	0.0257
		180	0.9893	0.0316
		300	0.9890	0.0346
Diffusion	$MR = a \cdot \exp(-kt) + (1 - a) \exp(-kbt)$	100	0.9796	0.0446
		180	0.9914	0.0292
		300	0.9920	0.0296

A drying model is considered optimal for accurately predicting moisture variation during drying when its (coefficient of determination) R<sup>2</sup> value closer to 1 with the least Root Mean Square Error (RMSE). The hot air drying and infrared have the lowest RMSE for the Logarithmic model of drying while for microwave drying Wang and Singh model is the most fitted with the least RMSE (Table 4-6).

**Table 6.** Models for different drying methods

Drying technique	Model name	Temperatures (°C)	Equations	R <sup>2</sup>	RMSE
Hot air drying	Logarithmic	105	$MR = a \cdot \exp(-kt) + b$	0.9961	0.0173
		110		0.9952	0.0195
		120		0.9943	0.0218
		130		0.9941	0.0220
		140		0.9932	0.0241
Microwave drying	Wang and Singh	100 W (61.66°C)	$MR = 1 + (at) + (bt^2)$	0.9929	0.0257
		180 W (68.66°C)		0.9893	0.0316
		300 W (78.93°C)		0.9890	0.0346
Infrared drying	Logarithmic	105	$MR = a \cdot \exp(-kt) + b$	0.9950	0.0175
		110		0.9981	0.0110
		120		0.9984	0.0101
		130		0.9991	0.0075
		140		0.9985	0.0100

### 3.5.3. Interpretation of Model Parameters in Drying Kinetics

Hot air drying was best described by the Logarithmic model, which showed the most suitable fit to the experimental data. The drying rate constant ( $k$ ) increased with temperature, indicating an accelerated drying process at higher temperatures. The parameter  $a$  exhibited slight fluctuations, reaching its maximum at 120 °C, suggesting that the initial moisture ratio factor was highest at this temperature. The parameter  $b$  showed a decreasing trend up to 120 °C, followed by a slight

increase, which may indicate that residual moisture content generally decreases with rising temperature but could increase at higher temperatures due to surface hardening or increased resistance to further moisture removal (Table 7).

Microwave drying was best represented by the Wang & Singh model, which provided the most suitable fit to the experimental data. The parameter  $a$  became more negative with increasing microwave power, indicating a faster initial drying rate, particularly at 300 W. The parameter  $b$  remained close to zero at lower power levels but turned positive at 300 W, suggesting a significant increase in non-linearity of the drying behavior. This trend is likely due to intensified internal moisture migration effects at higher microwave power levels (Table 7).

Infrared drying was best fitted by the Logarithmic model, which showed the most consistent performance across temperature variations. The drying rate constant ( $k$ ) increased steadily with temperature, indicating an enhanced drying rate at higher temperatures. The parameter  $a$  generally increased, reflecting a stronger initial reduction in moisture content as temperature rose. Meanwhile, the parameter  $b$  consistently decreased, suggesting a lower equilibrium moisture ratio and more effective overall drying at elevated temperatures (Table 7).

**Table 7.** Constant values of best fitted models for different drying techniques

Drying technique	Model name	Temperatures (°C)	Equations	k	a	b
Hot air drying	Logarithmic	105	$MR$	0.0121	0.9591	0.0950
		110	$= a$	0.0122	0.9693	0.0862
		120	$\cdot \exp(-kt)$	0.0143	0.9800	0.0787
		130	$+ b$	0.0153	0.9639	0.0797
		140		0.0191	0.9601	0.0931
Microwave drying	Wang and Singh	100 W (61.66°C)	$MR$	NA	-0.0093	0.0000
		180 W (68.66°C)	$= 1 + (at)$		-0.0090	0.0000
		300 W (78.93°C)	$+ (bt^2)$		-0.0143	$5.7259 \times 10^{-5}$
Infrared drying	Logarithmic	105	$MR$	0.0134	0.8708	0.1778
		110	$= a$	0.0141	0.8779	0.1537
		120	$\cdot \exp(-kt)$	0.0153	0.8820	0.1462
		130	$+ b$	0.0150	0.8691	0.1471
		140		0.0173	0.8972	0.1315

#### 3.5.4. Moisture Diffusivity in Iron Ore Briquette Sample

The iron ore briquette samples are highly porous, with micropores uniformly distributed across their surfaces. Moisture within these briquettes exists in several forms: bound water (held chemically or physically within the matrix), capillary water (contained in small pores), free water (located in larger pores), and surface moisture. Moisture migration occurs through various mechanisms, including liquid diffusion via interconnected pores (capillaries), vapor diffusion driven by vapor pressure gradients, and surface diffusion, where water moves along the walls of the pores.

Moisture diffusivity in a porous iron ore briquette describes how quickly moisture moves through the briquette's pore structure. It's a measure of the material's ability to allow moisture to penetrate and distribute within it during different drying processes. Higher diffusivity means moisture moves more easily and quickly through the briquette.

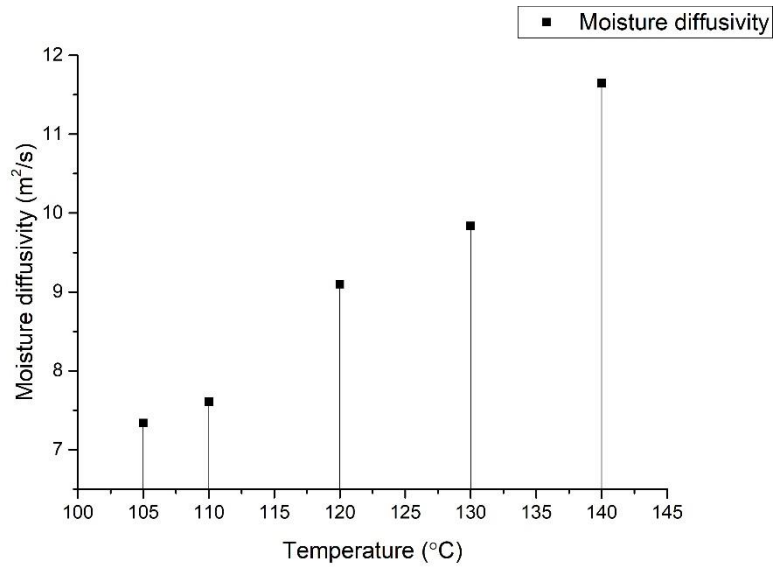


**Figure 18.** Graph between moisture diffusivity vs temperature after hot air drying

In hot air drying, heat is transferred from the hot air to the surface of the briquette primarily through conduction. During mass transfer, surface moisture evaporates first, followed by the movement of internal moisture toward the surface through diffusion driven by a concentration gradient. This process is mainly governed by the temperature gradient and internal moisture diffusion.

In hot air drying, the iron briquette sample is heated by the surrounding air. The material's temperature increases due to the difference between the surface temperature of the briquette and the hot air. The drying process is gradual, with moisture diffusivity increasing as the temperature rises from 105°C to 140°C. The breakage of inter-particle bonds in the iron ore briquette at 130°C (Figure 9) further contributes to the continuous rise in moisture diffusivity from 105°C to 140°C (7.33788 × 10<sup>-8</sup>, 7.60699 × 10<sup>-8</sup>, 9.09794 × 10<sup>-8</sup>, 9.83514 × 10<sup>-8</sup>, and 11.6445 × 10<sup>-8</sup> m²/s, respectively) (Figure 18). The iron ore briquette exhibited maximum strength at 120°C (3.680 N/mm²). However, as moisture diffusivity continued to increase and inter-particle bonds began to break, and that shows the decrease in strength upto 140°C (Figure 3).

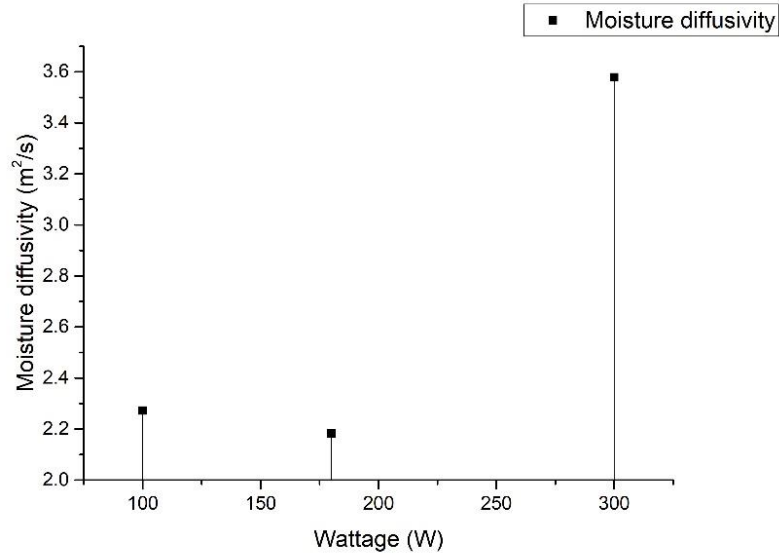


**Figure 19.** Graph between moisture diffusivity vs temperature after microwave drying

In microwave drying, heat is generated volumetrically through the dipole rotation of water molecules, resulting in internal heating of the briquette. Mass transfer occurs due to the rapid internal heating, which leads to increased internal pressure as moisture vaporizes within the briquette. This process promotes enhanced moisture migration from the core to the surface resulting in faster drying with minimal thermal gradients.

In microwave drying electromagnetic waves penetrate deeply into the iron ore briquette, heating the water vapor inside and pushing it out of the sample. This process can cause cracks on the surface of the briquette and potentially damage the sample. The moisture diffusivity at 100W ( $2.2727 \times 10^{-8} \text{ m}^2/\text{s}$ ) is higher compared to 180W because the electromagnetic waves penetrate more effectively at lower power. The compressive strength is highest at 100W ( $2.884 \text{ N/mm}^2$ ) (Figure 4) due to the gradual heating process, which helps preserve the inter-particle bonds in the iron ore briquette as compared to 180W and 300W, respectively (Figure 10-12). The oscillation of intermolecular bonds within the sample generates heat, which moves the water vapor toward the surface. At 180W a significant amount of energy is used to break the bonds resulting in a decrease in moisture diffusivity ( $2.1829 \times 10^{-8} \text{ m}^2/\text{s}$ ). This also led to a decrease in the strength of the iron ore briquette due to the breakage of its inter-particle bonds. However, at 300W, the bonds inside the briquette have already broken leading to an increase in moisture diffusivity to  $3.5778 \times 10^{-8} \text{ m}^2/\text{s}$  and results in the reduced strength of the briquette (Figure 19).

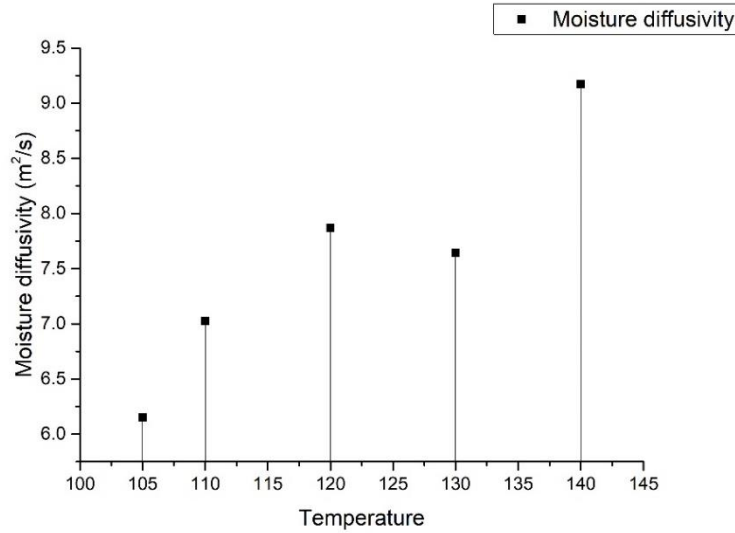


**Figure 20.** Graph between moisture diffusivity vs temperature after infrared drying

In infrared drying, heat transfer occurs when infrared radiation is absorbed at the surface of the briquette with conduction carrying the heat inward from the surface toward the core. The mass transfer process is similar to hot air drying but surface heating is more rapid in infrared drying. This method promotes evaporation and enhances the moisture gradient leading to more efficient drying.

In infrared drying energy packets in the form of photons are emitted directly onto the surface of the iron ore briquette, heating the sample without the need for a transfer medium. The moisture diffusivity increases from 105°C ( $6.1505 \times 10^{-8} \text{ m}^2/\text{s}$ ) to 120°C ( $7.86846 \times 10^{-8} \text{ m}^2/\text{s}$ ). However, at 130°C, significant energy is used to widen and weaken the inter-particle bonds, which reduces the amount of moisture removed and decreases moisture diffusivity to  $7.64326 \times 10^{-8} \text{ m}^2/\text{s}$ . This change in intermolecular bonding results from the rapid heating in infrared drying (Figure 20). As the inter-particle bonds continue to weaken and widen, the increased surface area within the sample enhances moisture diffusivity at 140°C ( $9.17137 \times 10^{-8} \text{ m}^2/\text{s}$ ). The strength of the iron ore briquette is highest at 120°C (4.195 N/mm<sup>2</sup>) and then decreases at 130°C and 140°C, respectively (Figure 5) due to the breakage of inter-particle bonds and continuous increase in moisture diffusivity of the iron ore briquette sample (Figure 16).

### 3.6 Study of Moisture Ratio and Time of Drying After Different Drying Techniques

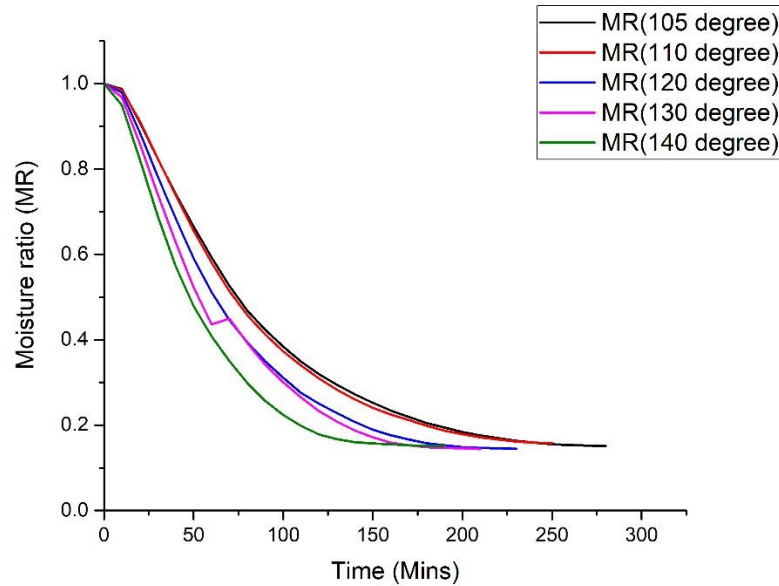


**Figure 21.** Graph between moisture ratio vs time after hot air drying

The iron ore briquette samples were dried at temperatures 105°C, 110°C, 120°C, 130°C and 140°C, respectively. The hot air drying of the iron ore briquette sample in beginning temperature increases gradually due to its high initial moisture content and low drying rate. As the process continues, the temperature rises more quickly, resulting in an increase in drying rate (Figure 21).

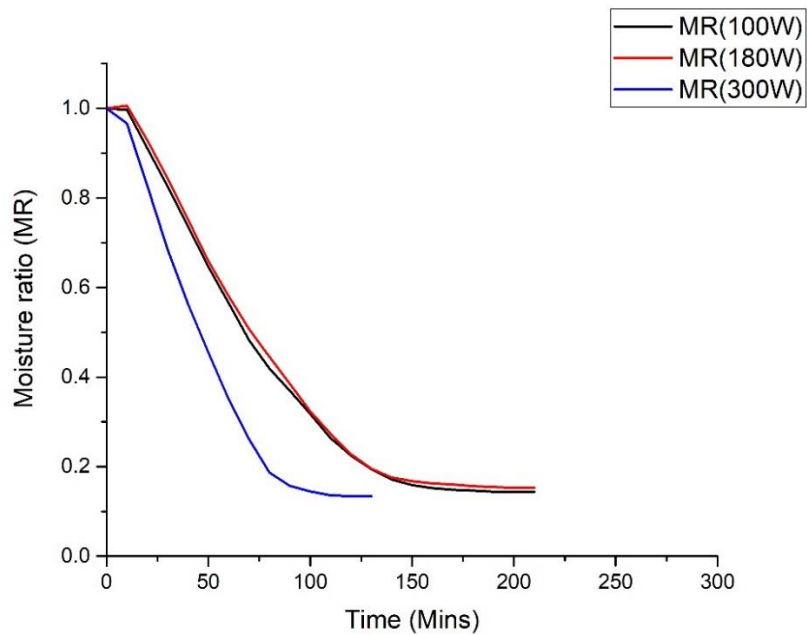


**Figure 22.** Graph between moisture ratio vs time after microwave drying

The iron ore briquette samples were dried at temperatures 105°C, 110°C, 120°C, 130°C and 140°C, respectively. During the initial stage of microwave drying, the sample's temperature rises slowly due to its high initial moisture content and low drying rate. However, as the drying process progresses, the temperature increases more rapidly, resulting in a higher drying rate (Figure 22).

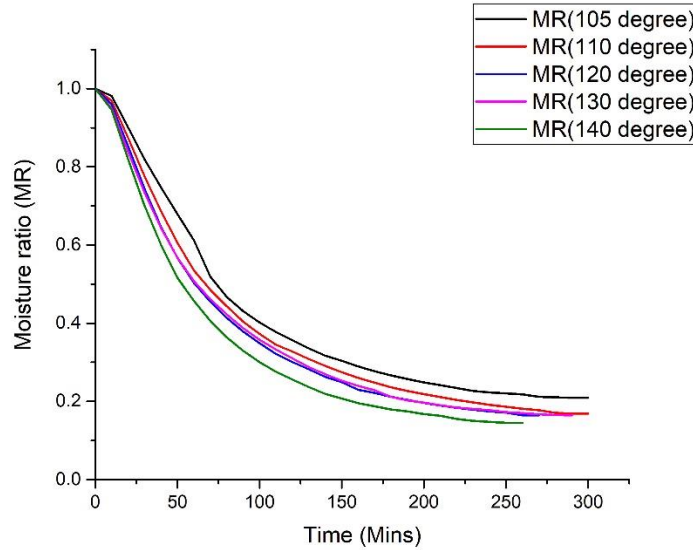


**Figure 23.** Graph between moisture ratio vs time after infrared drying

The iron ore briquettes were dried using microwave drying at power levels of 100W, 180W, and 300W, respectively. In the initial stage of infrared drying, the temperature of the sample increases slowly due to high initial moisture content and low drying rate. However, in the later stages of drying the sample temperature rises more rapidly, leading to a higher drying rate (Figure 23).

### 3.7 Determination of Porosity and Bulk Density

Iron ore briquette samples were prepared in batches of three at different temperatures, and the results were averaged. As the drying temperature increases, the porosity of the iron ore briquettes rises while the bulk density decreases (Table 8 and 9). The experiment followed ASTM standard B962-15 [25], which utilizes Archimedes' principle.

**Table 8.** Porosity and Bulk density for hot air drying and infrared drying after drying at different temperatures

Temperature (°C)	Hot air drying		Infrared drying	
	Porosity (%)	Bulk density (g/cm <sup>3</sup> )	Porosity (%)	Bulk density (g/cm <sup>3</sup> )
105	30	2.132	39.09	1.688
110	31.50	1.845	40.75	1.659
120	32.40	1.825	41.43	1.643
130	33.70	1.792	42.86	1.614
140	34.43	1.781	43.44	1.602

**Table 9.** Porosity and Bulk density for microwave after drying at different wattages

Wattage (W)	Power density (W/g)	Porosity (%)	Bulk density (g/cm <sup>3</sup> )
100	0.093	30.61	1.87
180	0.33	31.20	1.86
300	0.58	31.43	1.85

### 3.8 Energy Consumption for Drying in Hot Air, Microwave, and Infrared Technique

Three iron ore briquette samples each weighing a total of 480g, were prepared in batches and dried using various techniques. Approximately 13g of moisture was removed using these methods, as further drying led to the appearance of cracks. Hot air drying, with an energy consumption of 0.3 kW/h, produced briquettes with greater strength compared to those dried by microwave (Table 7). Although microwave drying is the most economical method in terms of energy consumption (0.2 kW/h), it results in the lowest strength (2.884 N/mm<sup>2</sup>) compared to hot air and infrared drying. Infrared drying achieved the highest strength (4.195 N/mm<sup>2</sup>) at 120°C, but it required the highest energy consumption (2.3 kW/h) among the drying techniques (Tables 10,11 and 12).

**Table 10.** Energy consumption in hot air drying

Drying temperatures (°C)	Energy consumption (KW/h)	Total time taken (Mins)	Electricity cost (Rs. /Kg)
105	0.2	90	1.25
110	0.2	75	1.25
120	0.3	60	1.87
130	0.4	60	2.50
140	0.5	45	3.12

**Table 11.** Energy consumption in microwave drying

Drying wattages (W)	Power density (W/g)	Energy consumption (KW/h)	Total time taken (Mins)	Electricity cost (Rs. /Kg)
100	0.093	0.2	70	1.25
180	0.33	0.3	35	1.25
300	0.58	0.4	20	1.27

**Table 12.** Energy consumption in infrared air drying

Drying temperatures (°C)	Energy consumption (KW/h)	Total time taken (Mins)	Electricity cost (Rs. /Kg)
105	1.8	60	11.25
110	2.0	50	12.50
120	2.3	50	14.37
130	2.5	40	15.62
140	2.7	40	16.87

## 4. Conclusion

The selected composition (LD sludge, flue dust, iron ore fines, cement, and bentonite) provides the maximum compressive strength for iron ore briquettes after drying. In microwave drying, moisture diffusivity is optimal at 100W, whereas it is low at 180W and very high at 300W. For both hot air and infrared drying, moisture diffusivity is low at 105°C, but the maximum strength is observed at 120°C due to medium moisture diffusion.

Agglomerates such as briquette, pellets and blocks are essential for effectively utilizing iron ore fines and metallurgical wastes. Infrared drying at 120°C yields the highest compressive strength (4.195 N/mm<sup>2</sup>) compared to microwave and hot air drying. Initially, drying methods show a slow increase in sample temperature due to high initial moisture content and low drying rates. When drying progresses the temperature rises quickly leading to a high drying rate, which can cause a decrease in compressive strength due to bond breakage at 130°C and 140°C. The drying rate at 120°C is moderate, contributing to high compressive strength and sample stability. At 105°C and 110°C, the low drying rates in hot air and infrared drying result in lower compressive strengths (2.220 N/mm<sup>2</sup> and 2.250 N/mm<sup>2</sup>, respectively).

The hot air and infrared drying have R<sup>2</sup> closer to 1 and the least RMSE in the case of the Logarithmic model of drying. While for microwave drying, Wang and Singh's model was the most fitted with the least error and R<sup>2</sup> closer to 1.

#### **Author contributions**

*Rishi Sharma: Investigation, Methodology, Writing—original draft, Paper modification and editing. D.S. Nimaje: Supervision, Formulation of research ideas, Project administration.*

#### **Declaration of Interests**

*The authors declare no competing interests*

#### **References**

- [1] S. M. Gandhi, B. C. Sarkar, Essentials of Mineral Exploration and Evaluation, Elsevier: Amsterdam, Netherlands, (2016) 23–52.
- [2] S. Chakravarty, P. Bhattacharyya, S. S. Chatterjee, B. N. Singh, The Utilization of Iron Ore Fines in Alternative Iron-Making Processes – An Indian Perspective. Proc. Fines, 2, (2000) 442–452.
- [3] S.P.E. Forsmo, P.O. Samskog, B. M. T. Björkman, A study on plasticity and compression strength in wet iron ore green pellets related to real process variations in raw material fineness, Powder Technology, 181(3) (2008) 321-330. <https://doi.org/10.1016/j.powtec.2007.05.023>
- [4] M. K. Mohanty, S. Mishra, B. Mishra, S. Sarkar, S. K. Samal, A novel technique for making cold briquettes for charging in the blast furnace. In IOP Conference Series: Materials Science and Engineering, 115(1) (2016) 012020. <https://doi.org/10.1088/1757-899X/115/1/012020>
- [5] D. Fernández-González, J. Piñuela-Noval, and Verdeja LF, Iron ore agglomeration technologies. Iron ores and iron oxide materials. Intechopen, Londres, (2018) 61-80.
- [6] B. B. Agrawal, K. K. Prasad, S. B. Sarkar, H. S. Ray, Cold Bonded Ore–Coal Composite Pellets for Sponge Ironmaking Part 2 Plant Trials in the Rotary Kiln, Ironmaking & Steelmaking Review, 28(1) (2001) 23–26. <https://doi.org/10.1179/030192301677812>

- [7] J. Aota, L. Morin, Cold bonded iron particulate pellets. U.S. Patent 6,676,725. B2, 2004, Jan13.
- [8] S. K. Kawatra, S. J. Ripke, Developing and Understanding the Bentonite Fiber Bonding Mechanism, *Miner. Eng. Review*, 14(6) (2001) 647–659. [https://doi.org/10.1016/S0892-6875\(01\)00056-5](https://doi.org/10.1016/S0892-6875(01)00056-5)
- [9] S. J. Ripke, S. K. Kawatra, Effect of Cations on Unfired Magnetite Pellet Strength. *Miner. Metall. Process*, 20(3) (2003) 153–159. <https://doi.org/10.1007/BF03403148>
- [10] M. Athayde, M. Cota, M. Covcevich, Iron ore pellet drying assisted by microwave: A kinetic evaluation, *Mineral processing and extractive metallurgy review*, 39(4) (2018) 266–275. <https://doi.org/10.1080/08827508.2017.1423295>
- [11] M. A. Nyembwe, Study of sinter reactions when fine iron ore is replaced with coarse ore, using an infrared furnace and sinter pot tests. Doctoral dissertation, University of Pretoria, (2012).
- [12] N. Tsioutsios, C. Weiss, J. Rieger, E. Schuster, B. Geier, Flame front progress in gas assisted iron ore sintering, *Applied Thermal Engineering*, 165(9) (2020) Article no.114554. <https://doi.org/10.1016/j.applthermaleng.2019.114554>
- [13] T. C. Souza Pinto, A. S. Souza, J. N. M. Batista, A. M. Sarkis, L. D. S. Leal Filho, T. F. D. Pádua, R. Béttega, Characterization and drying kinetics of iron ore pellet feed and sinter feed, *Drying Technology*, 39(10) (2021) 1359–1370. <https://doi.org/10.1080/08827508.2020.1747073>
- [14] A. L. Ljung, T. S. Lundström, B. D. Marjavaara, K. Tano, Influence of air humidity on drying of individual iron ore pellets, *Drying Technology*, 29(9) (2011) 1101–1111. <https://doi.org/10.1080/07373937.2011.571355>
- [15] S. Tan, J. Peng, H. Shi, Modeling and simulation of iron ore pellet drying and induration process with accurate bed void fraction calculation, *Drying Technology*, 34(6) (2016) 651–664. <https://doi.org/10.1080/07373937.2015.1070357>
- [16] P. Mbele, Pelletizing of Sishen concentrate, *Journal of the Southern African Institute of Mining and Metallurgy Review*, 112(3) (2012) 221–228.
- [17] Ye. Lian, Z. Jianliang, Yu. Jiyong, Runsheng Xu, D. Han, Evolution behavior and kinetic analysis of vacuum-extruded iron-rich dust briquette in blast furnace, *Journal of Cleaner Production*, 433 (2023) 139753. <https://doi.org/10.1016/j.jclepro.2023.139753>
- [18] H. Tang, Z. Yun, X. Fu, S. Du, Modeling and experimental study of ore-carbon briquette reduction under CO–CO<sub>2</sub> atmosphere, *Metals*, 8(4) (2018) 205.
- [19] M. A. Somerville, The strength and density of green and reduced briquettes made with iron ore and charcoal, *Journal of Sustainable Metallurgy*, 2(3) (2016) 228–238. <https://doi.org/10.1007/s40831-016-0057-5>
- [20] A. M. Bizhanov, S. A. Zagainov, Tests of briquettes for mechanical strength, *Metallurgist*, 65(3) (2021) 247–256.
- [21] L. M. Tavares, R. F. de Almeida. 2020. Breakage of Green Iron Ore Pellet, *Powder Technology*, 366 (2020) 497–507. <https://doi.org/10.1016/j.powtec.2020.02.074>
- [22] J. Shaohua, P. Singh, P. Jinhui, A. N. Nikoloski, L. Chao, G. Shenghui, R.P. Das, Z. Libo, Recent developments in the application of microwave energy in process metallurgy at KUST, *Mineral Processing and Extractive Metallurgy Review*, 39(3) (2018) 181–190. <https://doi.org/10.1080/08827508.2017.1401537>
- [23] C. Çırpar, Heat treatment of iron ore agglomerates with microwave energy. Master's Thesis, Middle East Technical University, Ankara, Turkey (2005).

[24] Z. Huang, L. Yi, T. Jiang, Y. Zhang, Hot airflow ignition with microwave heating for iron ore sintering, *ISIJ International*, 52(10) (2012) 1750-1756. <https://doi.org/10.2355/isijinternational.52.1750>

[25] ASTM Standard: B962-15 Standard test methods for density of compacted or sintered powder Metallurgy (PM) Products Using Archimedes' Principle, (2015).



JMIMB\_accepted\_manus